Cell Medicine, Part B of Cell Transplantation, Vol. 1, pp. 123–135, 2010
Printed in the USA.

2155-1790/10 $90.00 + .00
DOI: 10.3727/215517910X551053
www.cognizantcommunication.com

Monitoring of Liver Cell Transplantation in a Preclinical Swine Model Using Magnetic Resonance Imaging

Nathanael Raschzok,* Ulf Teichgräber,† Nils Billecke,* Anja Zielinski,* Kirsten Steinz,* Nora N. Kammer,* Mehmet H. Morgul,*‡ Sarah Schmeisser,* Michaela K. Adonopoulou,* Lars Morawietz,§ Bernhard Hiebl,¶ Ruth Schwartlander,# Wolfgang Rüdinger,** Bernd Hamm,† Peter Neuhaus,* and Igor M. Sauer*

*General, Visceral, and Transplantation Surgery, Experimental Surgery and Regenerative Medicine, Charité-Campus Virchow, Universitätsmedizin Berlin, Berlin, Germany
†Radiology, Charité-Campus Mitte, Universitätsmedizin Berlin, Berlin, Germany
‡Visceral, Transplantation, Thorax, and Vascular Surgery, Universitätsklinikum Leipzig, Leipzig, Germany
§Institute of Pathology, Charité-Campus Mitte, Universitätsmedizin Berlin, Berlin, Germany
¶Centre for Biomaterial Development and Berlin-Brandenburg Centre for Regenerative Therapies (BCRT), Institute for Polymer Research, GKSS Research Centre Geesthacht GmbH, Teltow, Germany
#Department of Materials, ETH Zurich, Zurich, Switzerland
**Cytonet GmbH, Weinheim, Germany

Liver cell transplantation (LCT) is a promising treatment approach for certain liver diseases, but clinical implementation requires methods for noninvasive follow-up. Labeling with superparamagnetic iron oxide particles can enable the detection of cells with magnetic resonance imaging (MRI). We investigated the feasibility of monitoring transplanted liver cells by MRI in a preclinical swine model and used this approach to evaluate different routes for cell application. Liver cells were isolated from landrace piglets and labeled with micron-sized iron oxide particles (MPIO) in adhesion. Labeled cells ($n = 10$), native cells ($n = 3$), or pure particles ($n = 4$) were transplanted to minipigs via intraportal infusion into the liver, direct injection into the splenic parenchyma, or intra-arterial infusion to the spleen. Recipients were investigated by repeated 3.0 Tesla MRI and computed tomography angiography up to 8 weeks after transplantation. Labeling with MPIO, which are known to have a strong effect on the magnetic field, enabled noninvasive detection of cell aggregates by MRI. Following intraportal application, which is commonly applied for clinical LCT, MRI was able to visualize the microembolization of transplanted cells in the liver that were not detected by conventional imaging modalities. Cells directly injected into the spleen were retained, whereas cell infusions intra-arterially into the spleen led to translocation and engraftment of transplanted cells in the liver, with significantly fewer microembolisms compared to intraportal application. These findings demonstrate that MRI can be a valuable tool for noninvasive elucidation of cellular processes of LCT and—if clinically applicable MPIO are available—for monitoring of LCT under clinical conditions. Moreover, the results clarify mechanisms relevant for clinical practice of LCT, suggesting that the intra-arterial route to the spleen deserves further evaluation.

Key words: Liver cell transplantation (LCT); Magnetic resonance imaging (MRI); Cell tracking; Micron-sized iron oxide particles (MPIO); Iron oxide particle

INTRODUCTION

Liver cell transplantation (LCT) is considered to be a potential alternative to orthotopic liver transplantation for the treatment of inherited and acquired liver diseases (10,11). Although several studies have demonstrated the safety and feasibility of this approach, clinical success remains limited and questions remain concerning engraftment, contribution to functional improvements, and the long-term survival of liver cell grafts (8,10,11,25).

Received July 17, 2010; final acceptance December 9, 2010. Online prepub date: December 22, 2010.
Address correspondence to Nathanael Raschzok, General, Visceral, and Transplantation Surgery, Experimental Surgery and Regenerative Medicine, Charité-Campus Virchow, Universitätsmedizin Berlin, Augustenburger Platz 1, 13353 Berlin, Germany. Tel: ++49 30 450 659078; Fax: ++49 30 450 559987; E-mail: nathanael.raschzok@charite.de *or* Igor M. Sauer, M.D., Ph.D., General, Visceral, and Transplantation Surgery, Experimental Surgery and Regenerative Medicine, Charité-Campus Virchow, Universitätsmedizin Berlin, Augustenburger Platz 1, 13353 Berlin, Germany. Tel: ++49 30 450 559002; Fax: ++49 30 450 559987; E-mail: igor.sauer@charite.de

Clinical LCT is generally performed by intraportal infusion, leading to occasional microembolization of transplanted cells in the liver (25). However, little is known about the mechanisms following cell application to the spleen, which is the main ectopic implantation site for LCT (10,11). A major obstacle in clinical studies exploring the outcome of LCT is the inability to noninvasively observe transplanted liver cells.

Magnetic resonance imaging (MRI) is currently the most promising approach for noninvasive tracking of transplanted cells (20). Cellular labeling with superparamagnetic iron oxide particles (SPIO) generates hypointense contrast on T2/T2*-weighted MRI sequences, enabling the in vivo detection of labeled cells by MRI (38). Initial clinical studies using nanometer-sized SPIO (Feridex, Bayer HealthCare) have shown encouraging results for imaging dendritic cells, neural stem cells, and islet cells (5). To track liver cells in a clinical setting, where clinical MR equipment and abdominal imaging sequences are mandated, high relaxivity of the contrast agent is of particular importance. Compared to nanometer-sized SPIO, micron-sized iron oxide particles (MPIO) show increased relaxivities given equal iron contents (32). Although not approved for clinical applications, several studies have successfully investigated MPIO for cellular imaging, reporting successful detections at a single cell level under experimental conditions (30,32). We have previously developed a protocol for labeling primary human hepatocytes with MPIO (27). In vitro, cells were detectable using 3.0 Tesla MRI and labeling had no adverse effects on the viability or metabolic activity of human liver cells. However, prior to possible translation of this method to the clinic, investigations with large-animal models are required. Such studies must address the detectability of MPIO-labeled liver cells under conditions of clinical abdominal imaging.

In this study, a swine model was chosen for preclinical investigation. Initially, MPIO labeling of porcine liver cells was investigated in vitro. Next, a threshold for detectability of labeled cells using abdominal 3.0 Tesla MRI was defined. Allogeneic liver cells were then transplanted via different routes into the liver or spleen and animals were investigated by repeated MRI up to 8 weeks after transplantation. The aim of this study was to investigate the safety and feasibility of noninvasive monitoring of LCT using MRI and to use this approach to evaluate different routes of application of liver cells.

MATERIALS AND METHODS

Animal Studies

Liver cells were isolated from 17 male landrace piglets (weight: 18–22 kg). Female minipigs ($n = 51$; Ellegard, Dalmose, Denmark; weight: 28–35 kg) were used as recipients. The animals were kept in the animal care facility of the Department of Comparative Medicine and Laboratory Animal Sciences, Charité Universitätsmedizin Berlin, and received humane care. Experiments were performed in accordance with the federal law regarding the protection of animals and approved by the relevant federal authorities for animal research (G-0110/08).

Study Design. Liver cells were transplanted using the following routes: 1) intraportal infusion into the liver, 2) direct injection into the splenic parenchyma, 3) intraarterial infusion into the spleen. Recipients were randomly allocated to the following groups: group 1, transplantation of MPIO-labeled liver cells ($n = 10$); group 2, transplantation of native liver cells ($n = 3$); and group 3, application of an equivalent number of pure particles ($n = 4$). Imaging and blood sampling were performed before transplantation and at days 2, 7, 14, 28, and 56 after transplantation. Animals of group 1 were sacrificed at each time point after transplantation, whereas all animals of group 2 were sacrificed at day 14. Animals of group 3 were sacrificed at days 2, 7, 14, and 28.

Operative Procedures. All animals were kept under general anesthesia during operative procedures. Liver and spleen were accessed through laparotomy. Animals of groups 1 and 2 underwent transplantation with a mean of $72.9 \pm 3.7 \times 10^6$ viable cells/recipient via all investigated administration routes. Intraportal cell application was performed using a three-lumen central line introduced into the portal vein. The cell suspension was applied under intermittent agitation through the distal 16-gauge branch at a rate of 20 million cells/min. Simultaneously, 30 ml of heparinized saline (500 U) was applied through the medial branch (22). For intrasplenic application, the spleen was exposed and 8 ml of cell suspension was injected directly into the parenchyma using an 18-gauge needle. The procedure was repeated three times in distant areas of the splenic parenchyma. Hemostasis was obtained by local compression with Tabotamp (ETHICON, Norderstedt, Germany) and electrocautery. For the intraarterial route, the gastroepiploic artery, a small branch of the splenic artery, was cannulated with an 18-gauge cannula. The spleen was flushed with 250 ml of heparinized saline (500 U), cells were infused at a rate of 20 million cells/min, and the artery was ligated thereafter. All animals were monitored for signs of medical complications after transplantation. For blood sampling, animals were sedated by ketamine/rompune.

Clinical Follow-up. Recipients were immunosuppressed with 250 mg IV methylprednisolone intraoperatively, cyclosporine at 10 mg/kg/day PO, and prednisolone at 1 mg/kg/day IM. Blood chemistry included cyclosporine blood trough levels, electrolytes, renal and liver profiles, iron metabolism parameters, and complete blood counts.

Liver Cell Processing

Porcine liver cells were isolated using a two-step collagenase perfusion technique as previously described (26). Cells were cultivated on collagen-coated 175-cm^2 culture flasks and six-well plates (Sarstedt, Nürnbrecht, Germany) with supplemented Williams' medium E (Biochrom AG, Berlin, Germany) (26). Superparamagnetic MPIO (Bangs Laboratories, IN, USA), with an average size of 1.63 μm, colabeled with Dragon-Green fluorochromes (480/520 nm), and encapsulated in divinyl benzene polymer microspheres as provided by the supplier, were used for labeling. Cells were incubated for 4 h at 60 particles/cell. Cells were washed twice with phosphate-buffered saline (PBS; PAA, Pasching, Germany), resuspended with 0.25/0.02% trypsin/ethylenediaminetetraacetate solution (Biochrom) (12), washed in PBS (4°C), and immediately transplanted. Samples were taken for in vitro studies and quality control.

In Vitro Studies

Liver cells from 5 of the 17 donors were divided into four groups (A: native/adherent; B: labeled/adherent; C: native/resuspended; D: labeled/resuspended) and cultivated for 6 days for in vitro studies.

Morphological Investigations. Particle uptake and retention were evaluated in six-well plates at days 2, 4, and 6 after labeling by light microscopy. For morphological investigation, cells from groups C and D were recultivated in the SlideReactor, a hollow fiber-based bioreactor system suitable for real-time morphologic analysis of cultured cells (29).

Enzyme Leakage and Synthesis Activity. Biochemical parameters were analyzed from the culture supernatants from days 2 to 6 on a daily basis. Aspartate aminotransferase (AST) and alanine aminotransferase (ALT) enzyme activities were measured (NobiFlow GOT-IFCC and GPT-IFCC). Urea formation was detected via an enzyme-based detection kit (NobiFlow Harnstoff-UV, all HITADO, Möhnesee, Germany). Protein concentration was determined from whole cell lysates (Interchim, Mont Lucon, France) on day 6 and enzyme levels were normalized to protein. All measurements were performed at least twice.

Phantom Preparation for In Vitro MRI. A dilution series from 5,000 to 200,000 labeled and native liver cells was prepared in 1.8 ml cryotubes (Sarstedt). Cell suspensions were layered on 2% agarose (Eurogentec, Seraing, Belgium) with 0.2 mmol/L gadolinium (Dotarem, Guerbet GmbH, Sulzbach, Germany). Cryotubes were fixed in gelatin and placed in a 50-cm-diameter water bowl for MRI. Experiments were repeated three times.

Imaging Studies

During imaging, animals were intubated and maintained on ketamine/rompune sedation and spontaneous breathing. For temporary breath hold, animals received a propofol bolus and were hyperventilated mechanically. Imaging was performed in the prone position.

MRI. In vivo MRI was performed using a 3.0 Tesla MR scanner (Signa 3T94, General Electrics Healthcare, Milwaukee, WI, USA) and a 4-channel torso phased array coil. Details of sequences used are summarized in Table 1 (9). Gadolinium was infused at a flow rate of 2 ml/s in order to enhance the image background of T1-weighted liver acquisition with volume acceleration (LAVA) images for detection of signal voids in the liver. The phantom was investigated using the same scan parameters. For MR mapping, liver lobes were perfused with formalin and investigated ex vivo under the same conditions.

CTA. Computed tomography angiography (CTA) was performed at day 7 following cell or particle application. A 64-row CT scanner (Light speed VCT, General Electric Healthcare) was used for imaging and Xenetix 350 (Guerbet GmbH, Sulzbach, Germany) was applied as contrast agent.

Imaging Analysis. Images were analyzed using OsiriX DICOM Viewer [Version 3.6.1, Osirix Foundation, Geneva, Switzerland (http://www.osirix-viewer.com)]. Signal-to-noise ratio (SNR) was measured three times. SNR was calculated as [signal – noise (mean)]/noise (SD).

Assessment of Liver Cell Engraftment

Tissue was sampled systematically from liver and spleen of animals from all groups. To guarantee an exact correlation with MRI data, samples were taken following ex vivo MRI mapping at days 2, 7, and 14 after the intraportal application of labeled cells. Tissue was frozen or fixed in formalin.

Morphometric Evaluation. Tissue sections underwent hematoxylin and eosin (H&E) or Perl's Prussian blue staining. For immunohistochemistry, sections were stained with mouse monoclonal cytokeratine (CK) 18 antibody (ab668; Abcam, Cambridge, UK) or mouse monoclonal macrophage antibody (ab22506; Abcam). Fluorescence in situ hybridization (FISH typing) was performed using Porcine IDetect Chromosome Y probes (548/573 nm) (IDPR1065; ID Labs Inc., London, ON, Canada). Slides were analyzed with a combined light and fluorescence microscope (Axio Imager M1, Zeiss, Jena, Germany) or a confocal microscope (Leica SP5, Leica, Wetzlar, Germany). Ultrathin sections were stained with 4% uranyl acetate and Reynolds lead citrate

Table 1. MRI Sequences and Parameters

Sequence	TR/TE (ms)	FA	ST (mm)	FOV (cm)	BW (kHz)	Matrix	Additional Parameters
3D T1-weighted LAVA	3.464/1.6	10°	3/1.5	34 × 32	100	256 × 256	Breath hold, gadolinium enhanced
T2-weighted fast spin echo	9,090/105	90°	6	30 × 27	41.67	320 × 256	Respiratory triggering
T2*-weighted	500/30	20°	3	34 × 32	122.1	256 × 256	Breath hold

MRI was performed with a 3.0 T MR scanner using a 4-channel torso phased array coil. Repetition time (TR), echo time (TE), flip angle (FA), slice thickness (ST), field of view (FOV), receiver bandwidth (BW), liver acquisition with volume acceleration (LAVA).

and imaged using an electron microscope (EM 906, Zeiss).

Molecular Confirmation. The sex-determining region Y (SRY) gene and β-actin gene DNA were investigated by PCR. Genomic DNA was isolated from frozen liver tissue (Nucleospin Tissue, Macherey-Nagel, Düren Germany). Tissue isolates were tested for male cells utilizing primer specific to the SRY (sense 5′-CGGG CAAGGCAGACCCCAAG-3′; anti-sense 5′- AGGG GAAGGCCGAGCCGTAG-3′). β-Actin-specific primers (sense 5′-CTGGACTTCGAGCAGGAGATG-3′; antisense 5′-TGTCGACGTCGCACTTCATG-3′) were used for controls. The PCR protocol consisted of an initial step at 94°C for 3 min, followed by 60 cycles: denaturation at 94°C for 30 s, annealing at 61.4°C (SRY gene) or 59.7°C (β-actin) for 30 s, and elongation at 72°C for 1 min. Cultivated and resuspended male donor cells were used as a positive control for the SYR gene; liver tissue from female animals receiving pure particles served as negative control.

Statistical Analysis

All data are expressed as mean ± SEM. Statistical analysis (one-way ANOVA with subsequent post-hoc pairwise comparisons, chi-square test, two-tailed Student's *t*-test, Wilcoxon test, Bonferroni correction) was performed using Microsoft Excel for Mac 2004 (V11.3.6, Microsoft Corporation, Redmond, WA, USA) and SPSS version 15 for Windows (SPSS Inc., Chicago, IL, USA). A value of $p < 0.05$ was considered statistically significant.

RESULTS

Labeling of Porcine Liver Cells With MPIO Had no Adverse Effects With Cells Remaining Stable In Vitro

Liver cells were cultivated in adhesion for 24 h prior to transplantation. Mean viability after liver cell labeling and preparation for transplantation was 46.8 ± 2.4%. Mean particle uptake was 20 ± 1 particles/cell with a labeling efficiency of 94.6 ± 0.8%. Observations in the SlideReactor indicated no differences in morphology between native and labeled cells (Fig. 1A, B). Labeling was not affected by resuspension and remained stable throughout the investigation period of 6 days (Fig. 1C). As parameters for cellular integrity, leakage of the liver-specific enzymes AST and ALT was investigated. By culture day 2, both enzyme concentrations were higher for resuspended cells compared to continuously adherent cells, due to previous trypsin treatment for enzymatic resuspension. Throughout the rest of the culture period, enzyme levels and urea formation remained similar for all groups (Fig. 1D–F). These experiments showed that MPIO labeling did not affect porcine liver cells, similar to our previous findings with primary human hepatocytes (27).

Aggregates of MPIO-Labeled Cells Induced Signal Extinctions That Were Detectable Using Abdominal 3.0 Tesla MRI

To determine the in vitro threshold for the detection of MPIO-labeled liver cells under conditions of abdominal MRI, dilution series of labeled and native cells were investigated using a whole-body coil. Labeled cells induced a hypointense signal on T1- and T2-weighted MR images (Fig. 1G). The SNR of labeled cells was significantly lower compared to native cells from a number of at least 10,000 cells (Fig. 1H), defining an aggregate of labeled cells necessary for the induction of signal changes detectable by abdominal 3.0 Tesla MRI.

Transplantation of Labeled Cells Induced Signal Voids in the Liver

The gadolinium-enhanced, T1-weighted, transversal LAVA gradient echo sequence was used for liver imaging. On pretransplant images, the liver parenchyma was homogenous (Fig. 2A). Following intraportal application of labeled cells, signal voids appeared in the periphery of the liver (Fig. 2B, C). Signal voids were detected in 9 out of 10 animals and showed no change in number or localization from day 2 to day 56 after transplantation. CTA at day 7 following transplantation excluded artifacts caused by entrapped air and showed no perfusion inhomogeneities or morphological correlations for signal voids (Fig. 2D). In contrast, application

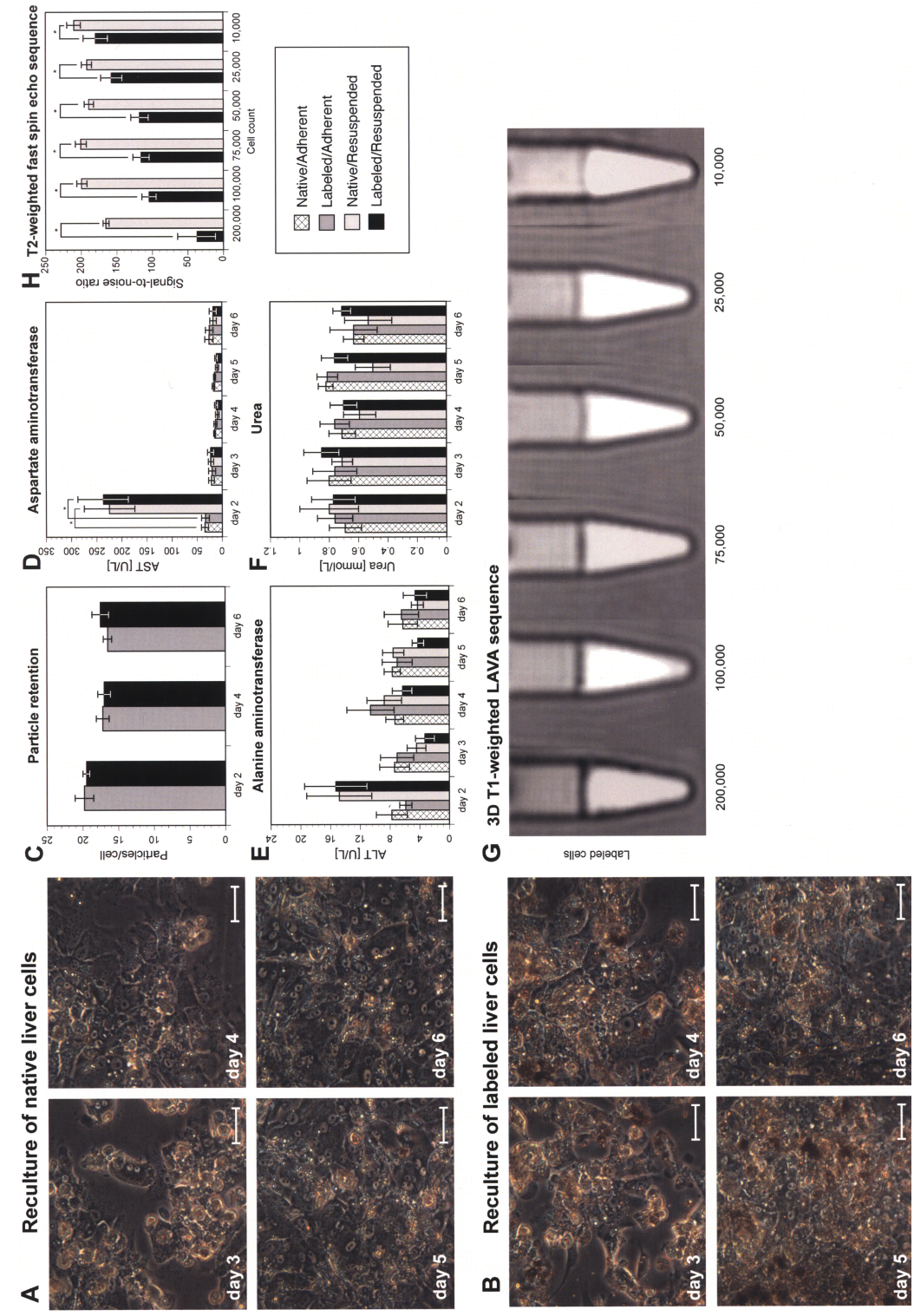

Figure 1. In vitro characterization of micron-sized iron oxide particle (MPIO)-labeled porcine liver cells. Native and labeled cells cultivated in the SlideReactor showed no differences in morphology (scale bars: 100 μm) (A, B). Labeling had no adverse effects on particle load (C), cellular integrity (D, E), or metabolic activity (F) (one-way ANOVA and Student's *t*-test with Bonferroni correction, $^*p < 0.05$). A transient increase of levels of aspartate aminotransferase (AST) was found at day 2 following enzymatic resuspension. Experiments were repeated with cells from five individual donors. Threshold for detection of MPIO-labeled liver cells by abdominal MRI. Dilution series of labeled and native cells investigated by 3D T1-weighted liver acquisition with volume acceleration (LAVA) sequences (G). The signal-to-noise ratio (SNR) of labeled cells was significantly lower compared to native cells from at least 10,000 cells (H) (two-tailed Student's *t*-test, $^*p < 0.05$).

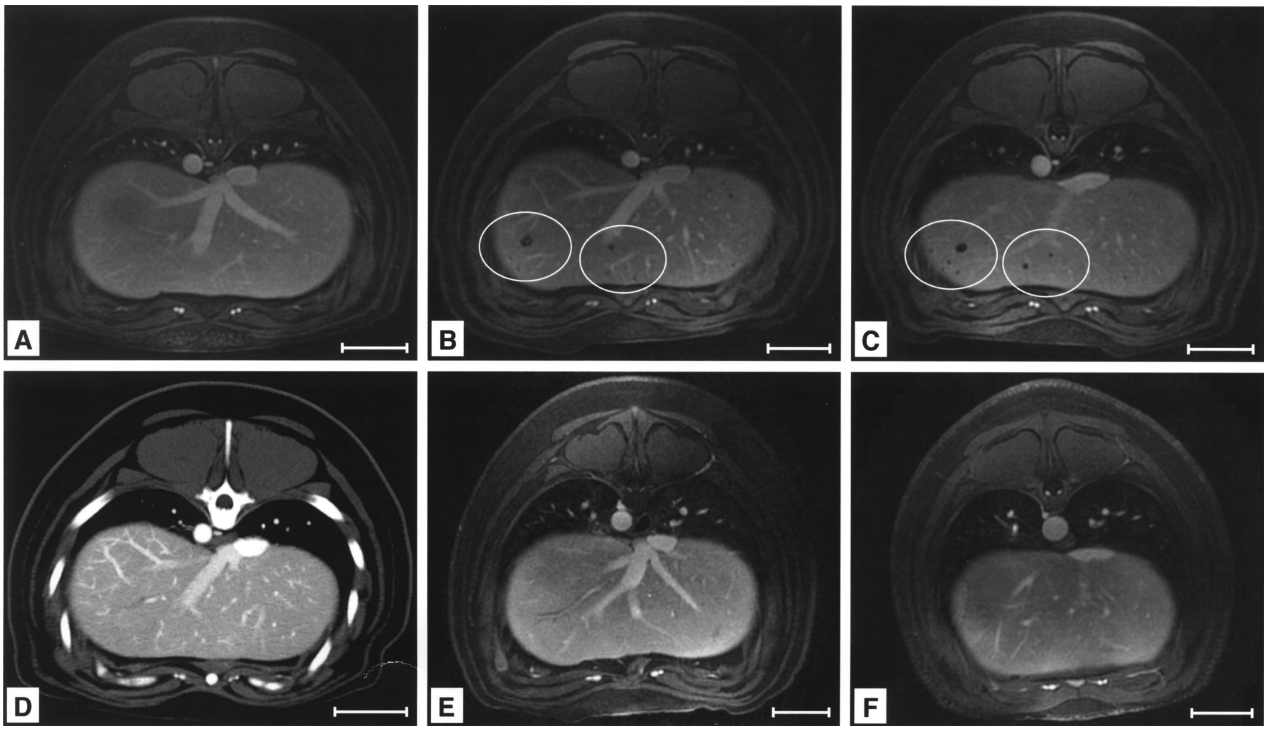

Figure 2. Detection of signal voids by MRI after intraportal liver cell transplantation (LCT) of labeled cells. In vivo MRI of the same animal before LCT (A), 7 days (B), and 14 days (C) after intraportal infusion of MPIO-labeled liver cells showed signal voids after application of MPIO-labeled cells (3D T1-weighed angio LAVA). Computed tomography angiography (CTA) of the same animal excluded artifacts due to entrapped air within the liver parenchyma and showed no perfusion inhomogeneities (D). Application of native cells (E) or pure particles (F) in control groups induced no signal voids (day 7 after application). Scale bars: 50 mm (A–F).

of native cells or pure particles induced no change in homogeneity of the liver parenchyma (Fig. 2E, F).

Signal Voids Were Caused by Labeled Cells Embolized in Distal Portal Branches

Histological examinations of tissue from hypointense areas (Fig. 3A) revealed microthrombi of Perl's Prussian blue-positive cells wedged into peripheral branches of the portal vein (Fig. 3B). Hypointensity was caused by the presence of MPIO, which was validated by electron microscopy (Fig. 3C). FISH typing revealed donor cells as the origin of the microthrombi (Fig. 3D). At day 14 after transplantation, microthrombi were infiltrated with macrophages, colocalized with most of the particles from ingested donor cells (Fig. 3E). FISH-positive cells were mainly localized in the periphery of microthrombi and were negative for the hepatocyte-specific CK 18 at day 14 following transplantation (Fig. 3F), presumably due to ingestion of donor cells by macrophages resolving the microthrombus. Portal vein radicles were not entirely occluded and no signs of abnormal changes in liver parenchyma were found following histopathological examinations. Individual FISH-positive, labeled donor cells (data not shown) were found in periportal areas of $52.4 \pm 5.8\%$ of liver sections/recipient, not reaching the threshold for detectability given the applied MRI protocol. MPIO labeling did not interfere with integration of donor cells into the liver parenchyma, because similar numbers of FISH-positive native cells were found to be engrafted in periportal areas compared to labeled cells. PCR for the male cell-specific SRY gene verified the presence of male donor cells. Microembolization was not caused by MPIO labeling, because samples from animals receiving native cells exhibited similar microthrombi. In control groups with the intraportal application of pure particles, microthrombi were not found, excluding that signal voids were induced by macrophages having taken up circulating MPIO and accumulated in the portal periphery.

Intrasplenically Transplanted, Labeled Liver Cells Were Engrafted in the Spleen and Led to Distinct Areas of Hypointensity

For imaging of the spleen, the T2-weighted fast spin-echo sequence was used. Intrasplenic injection of MPIO-labeled cells induced distinct areas of hypointensity around the three puncture sites in the spleen of 9 out of 10 recipients (Fig. 4A). Localization and the number of

hypointense areas were stable throughout the observation period. CTA excluded hematomas at injection sites, which would have similar MRI appearances (Fig. 4B). Staining for CK-18 revealed liver cells that were engrafted in clusters within the splenic parenchyma (Fig. 4C). Under electron microscopy, MPIO was apparent within the liver cells, indicating particle retention following the transplantation of labeled cells (Fig. 4D). Histological evaluation of the liver of the same animals identified small numbers of Perl's Prussian blue-positive cells within liver plates (Fig. 4E). The application of native liver cells induced no detectable signal changes of the spleen on MRI (data not shown), but injection of pure particles led to hypointense areas similar to MPIO-labeled cells (Fig. 4F).

Intra-arterially Infused Cells Were Carried to the Liver and Engrafted in Liver Plates With Significantly Fewer Microembolizations

Intra-arterial infusion of MPIO-labeled cells as well as native cells or pure particles induced no detectable signal changes in the spleen (Fig. 5A). Immunohistological evaluation identified small numbers of single CK-18-positive cells, mainly localized in splenic red pulp (Fig. 5C). Because the blood flow to the liver had not been blocked, cells did not seed in the splenic pulp and were cleared into the portovenous system. Under MRI, the liver had a homogeneous appearance after intra-arterial infusion of labeled cells, with signal voids found in only two cases (Fig. 5D). Evaluation with Perl's Prussian blue (Fig. 5E) showed MPIO-labeled donor cells engrafted in periportal areas of liver plates in 43.7 ± 11.43% of liver sections/recipient. FISH typing (Fig. 5F) and PCR (Fig. 6A) verified the presence of donor cells. Cell engraftment after intra-arterial infusion and subsequent translocation to the liver was similar to that following intraportal application (Fig. 6B), but histological findings confirmed significantly less frequent microembolization detectable by MRI after LCT via the intra-arterial route ($p = 0.005$).

Application of MPIO-Labeled Liver Cells Had no Adverse Clinical Effects

Splenic vein thrombosis was found in two cases following intrasplenic injection; thrombosis of main portal branches was found in 30% of the recipients following

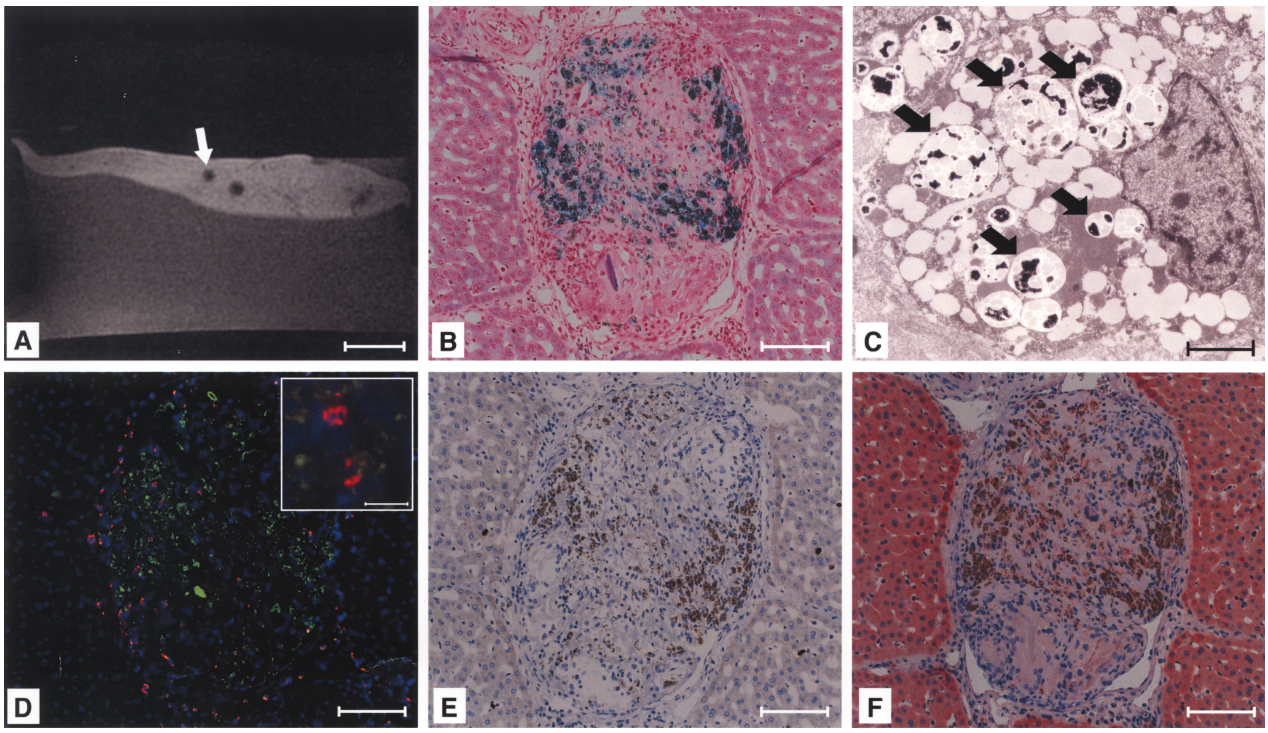

Figure 3. Signal voids in the liver were caused by microembolization of labeled cells. Histology revealed intraportal microthrombi as morphological correlations of signal voids (A, arrow), containing Perl's Prussian blue-positive (B), MPIO-labeled cells (C, signed with arrows). The presence of Y-chromosomes within the embolus confirmed MPIO-labeled donor cells as the origin of microthrombi (red: Y-chromosome, blue: nuclei, green: MPIO) (D). The embolus was infiltrated with macrophages (E) and labeled cells were not positive for cytokeratine (CK)-18 at day 14 after transplantation (F). Scale bars: 20 mm (A); 100 µm (B, D–F); 2.5 µm (C), 20 µm (D, inlay).

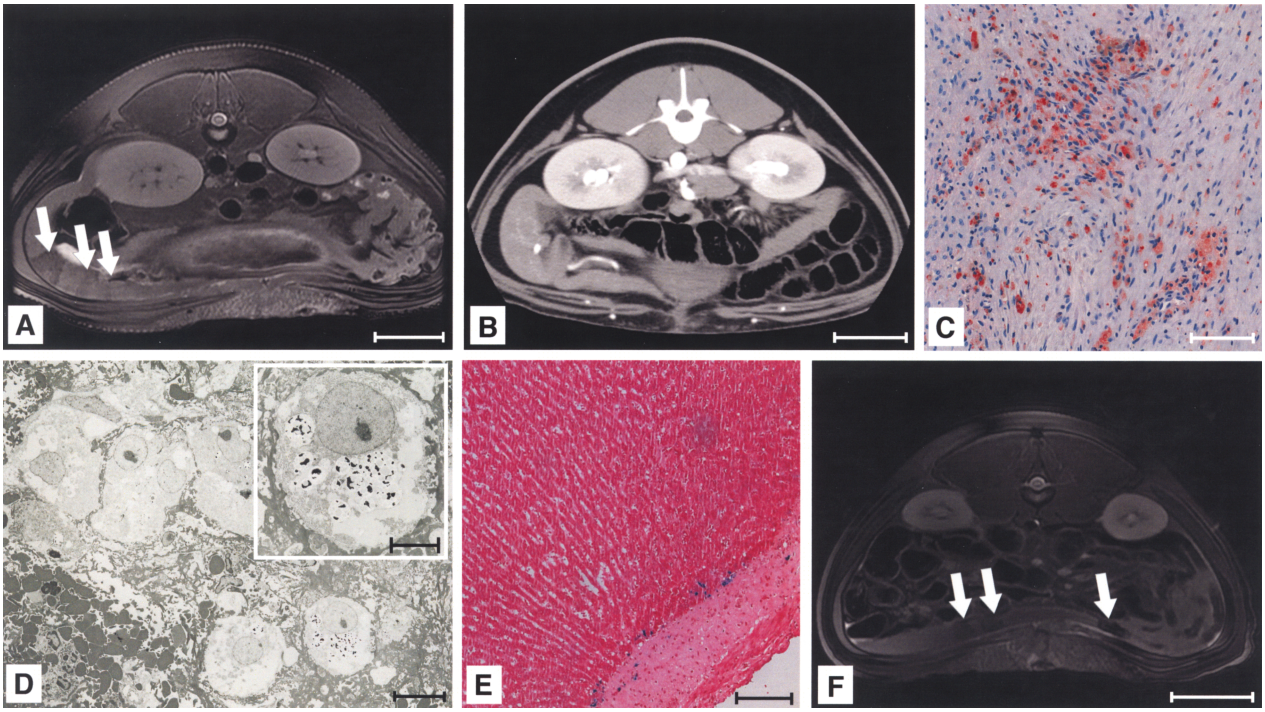

Figure 4. Intrasplenic LCT led to distinct areas of hypointensity in the spleen. Engraftment of intrasplenically injected, labeled cells induced distinct areas of hypointensity (signed with arrows) (A, day 14 after transplantation). CTA excluded hematoma at the injection site (B). Immunohistology showed clustering of liver cells engrafted within the spleen, positive for CK-18 at day 14 after transplantation (C). Electron microscopy confirmed particle retention within engrafted liver cells (2 days after transplantation) (D). The liver showed small numbers of Perl's Prussian blue-positive cells, mainly localized in the adventitia of portal vessels (E). Application of particles caused comparable areas of hypointensity (F). Scale bars: 50 mm (A, B, F); 100 µm (C, E); 10 µm, 5 µm (D, inlay).

intrasplenic or intraportal application. In contrast, intraarterial infusion caused no thrombosis. Signs of infection due to particle applications were not observed. Aside from transiently increased liver enzymes following surgery, the investigated parameters indicated no effects on liver physiology on account of either particles or labeled cells. Evidence for the degradation of MPIO or iron metabolism impacts were not observed, with blood ferritin and iron levels not increased by labeled cells as compared to native cells (data not shown). Histologically, no signs of malignant transformation in the area of the engrafted cells were observed. Investigated parameters revealed no systemic effects of MPIO-labeled liver cells compared to native cells or pure particles.

DISCUSSION

The inability to track transplanted cells in vivo in an efficient, noninvasive manner is a major obstacle for the clinical translation of cellular therapies in regenerative medicine. Multimodal or molecular imaging strategies are of great promise for evaluating the functional properties of transplanted cells, but they remain distant from clinical application (6,20). In contrast, cell tracking by MRI has already reached clinical trials and protocols for labeling of human liver cells with MRI contrast agents are available (5,21). We aimed to investigate the feasibility of monitoring LCT in a swine model with MPIO-labeled liver cells using clinical MRI.

According to our protocol for labeling of human liver cells with MPIO (27), we performed labeling in adhesion culture, which necessitated enzymatic resuspension of cells for transplantation. Enzymatic detachment is known to have negative effects on liver cells and is considered to be responsible for the low viability of MPIO-labeled cells (less than 50%), which would be too low for clinical transplantation (11). Further improvements of the labeling protocol as well as up-scalable purification procedures are necessary to prepare MPIO-labeled liver cells with higher viability. However, analogous to our previous studies using human liver cells, in vitro investigations showed satisfying recovery of liver cells from the labeling and resuspension procedure.

A 3.0 Tesla MR scanner, routinely available in most hospitals, was used for imaging and sequences with

shortened scan times were applied to generate high spatial resolution images with reduced respiratory motion artifacts (9). Under these conditions, the threshold study revealed that at least 10,000 MPIO-labeled cells were necessary to induce signal loss that was detectable by abdominal MRI in vitro. This was attributed to the lower field strength applied in our preclinical setting compared to experimental studies (30,32), because a decrease in field strength leads to a reduction in sensitivity, contrast, and resolution (18). Unlike our previous in vitro experiments, we used a whole-body coil, increasing the field of view by decreasing image resolution. Moreover, the T2*-weighted sequence, which usually yields the best results for imaging labeled cells, was not applicable because of the lengthy breath hold periods needed for abdominal MRI at 3.0 Tesla. Barnett et al. had previously achieved single cell detection in a swine model of islet cell transplantation (2). In order to obtain strong labeling combined with immunoprotection, they embedded islets in alginate with Feridex particles, containing 81 ng of iron per capsule. Compared to an MPIO-labeled liver cell, (i.e., about 20 pg) this is 4000-fold more iron, inducing significantly stronger disruption of the magnetic field. Therefore, MPIO-labeling should enable the detection of liver cell aggregates as opposed to single cells in the clinical setting of LCT, contrary to expectations raised by previous small animal studies on cell tracking by MRI (4,15,30). These results underline the advantages of using MPIO for monitoring after cell transplantation under conditions of clinical abdominal MRI. Using clinically approved SPIO, which are known to induce lower signal extinctions at similar iron load compared to MPIO (32), the detection threshold of labeled cells or cell aggregates could be even higher, which would lead to presumably even worse detectability and the impossibility to evaluate cellular processes on a detailed level in vivo. This assumption is in line with recent results from a study of Shi et al. on tracking of SPIO-labeled mesenchymal stem cells (MSCs) using 1.5 Tesla MRI after intraportal transplantation in a swine model of acute liver injury (31). They observed general decrease of signal intensity of the recipient liver 6 h

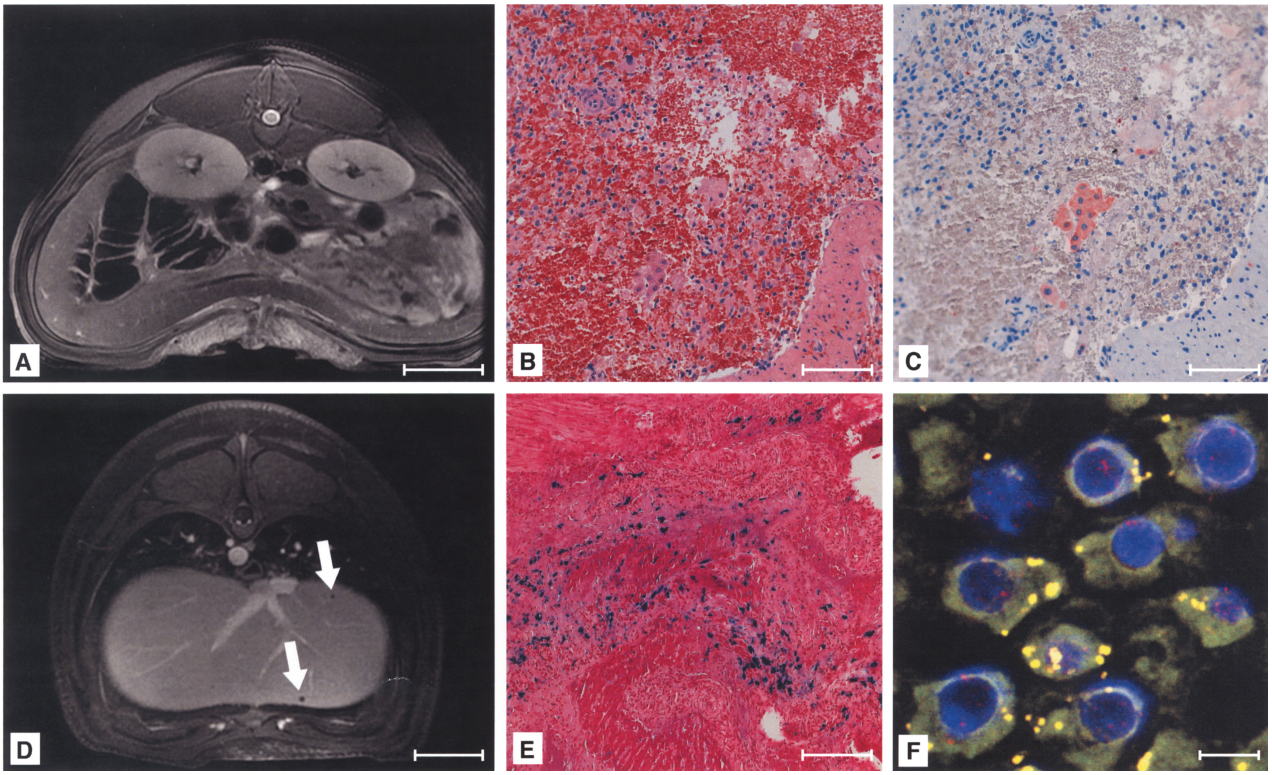

Figure 5. Intra-arterial transplanted cells were carried to the liver and engrafted in periportal areas. MRI showed no detectable signal changes in the spleen after intra-arterial application of labeled cells (A). Only a small number of liver cells were retained in the spleen (H&E: B, CK-18: C). Microthrombi within the liver were not detectable by MRI after cell application via this route, with the exception of two cases (D), but Perl's Prussian blue-positive cells were engrafted within the periportal areas of the liver (E). Fluoresence in situ hybridization (FISH) typing confirmed the presence of male cells within the liver after intra-arterial infusion and portovenous translocation (red: Y-chromosome, blue: nuclei, green: MPIO) (F). Scale bars: 50 mm (A, D); 100 μm (B, C, E); 10 μm (F).

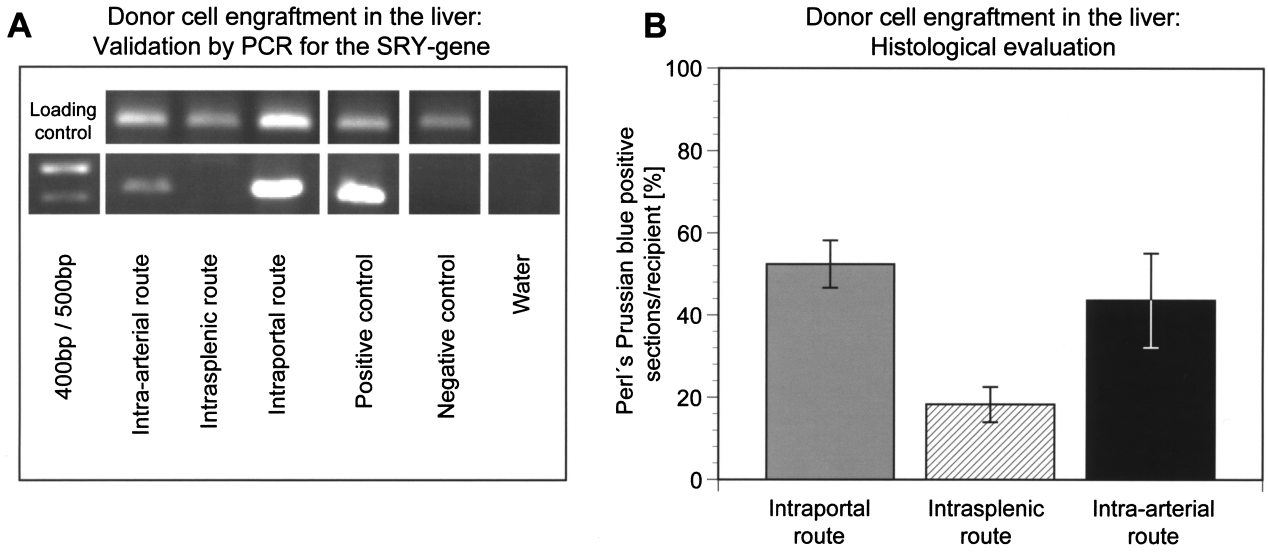

Figure 6. Comparison of cell engraftment in the liver after application via different routes. PCR for the sex-determining region Y (SRY) gene confirmed the presence of male cells in liver samples following intraportal or intra-arterial LCT (A). Cell engraftment was evaluated at day 14 after transplantation ($n = 6$ animals per group). The number of Perl's Prussian blue-positive liver sections/recipients was not significantly different (chi-square test, $p = 0.441$) after intraportal infusion compared to intra-arterial infusion into the spleen and portovenous translocation to the liver (B). Cell translocation and engraftment was significantly lower following intrasplenic injection compared to intraportal infusion ($p = 0.007$) or intra-arterial infusion ($p = 0.036$).

after transplantation of labeled MSCs that gradually approached to normal levels during the follow-up, presumably due to cell division or break down of particles with signal decreasing below detection threshold.

We have to emphasize that the particles used in our study are not clinically approved. Possible challenges for clinical approval may arise due to the fact that nondegradable particles such as the polymer-coated MPIO are likely to persist in the body of the recipient, which in turn would not occur when using biodegradable SPIO. However, independent of further clinical applicability, MPIO should be useful for noninvasive elucidation of cellular processes of LCT in ongoing preclinical large animal studies.

In order to show the feasibility of this approach, we used MPIO-labeled cells to evaluate different routes of administration for liver cells with MRI monitoring. Clinically, both the liver and spleen are considered primary implantation sites, with consensus on the liver as the most appropriate place for the long-term function of liver cell grafts (11). For successful integration into liver plates, transplanted cells need to cross the sinusoidal barrier following accumulation in periportal vessels and hepatic sinusoids, with occasional microthrombi formation (13). Our study shows that MRI enables visualization of microembolization by MPIO-labeled liver cells, whereas differentiation between labeled donor cells and macrophages that infiltrated the microthrombus was not possible. Previously, these microthrombi have not been detected with noninvasive methods (25), because CTA is not adequate for their visualization. Microembolization occurred in almost all animals following intraportal LCT, the route most commonly utilized in clinical LCT. Cells were transplanted without prior damage to the liver and were thus infused into an intact vascular bed, similar to that of patients suffering from inborn metabolic liver disease. As recently demonstrated by Quaglia et al., microembolization is not an uncommon event in these patients after intraportal LCT (25). Furthermore, microembolization has been observed in large-animal models without a preparative regimen prior to intraportal LCT (1,17,22,37). It might be worth considering whether embolized cells may contribute to temporary recovery of metabolic function after LCT (25). However, it is evident that these cells do not engraft in the recipient liver parenchyma, a step required for the definitive cure of metabolic liver disease. Our data confirm that microembolization is frequent following intraportal cell application, and we assume that this mechanism is, among others, responsible for the limited outcome of clinical LCT. To avoid embolization, enhance engraftment, and induce proliferation of transplanted cells, strategies such as partial portal embolization or irradiation are investigated (7,39). An alternative route for cell delivery to the liver could be the hepatic artery, which was recently used for transplantation of human fetal liver-derived stem cells (16). For clinical studies on the improvement of liver cell engraftment and possible comparison of both routes for cell infusion to the liver, transplantation of a fraction of MPIO-labeled cells and follow-up MRI monitoring

could be of major interest. The absence of signal voids should exclude the microembolization of transplanted cells of a certain aggregate size and indicate successful cell engraftment.

The spleen was previously considered to be the ideal ectopic implantation site for hepatocytes, with possible advantages for patients with chronic liver disease, where damaged liver architecture prevents hepatocyte engraftment (11). For the administration of liver cells to the spleen, two routes are possible, namely intrasplenic injection and intra-arterial infusion. It is well known in rodents that cells may be carried to the liver following intrasplenic application (24), but little attention has been paid to this phenomenon in the clinic, although donor cell engraftment in the liver after LCT via the splenic artery has been demonstrated (3,36). Interested in the fate of liver cells after transplantation into the spleen, we investigated both routes using MRI. We observed hypointense areas in the spleen following intraparenchymal injection of labeled cells. Similar MR images were obtained following the injection of pure particles, demonstrating the infeasibility of distinguishing between labeled cells and scattered particles, a requirement for monitoring cell loss after transplantation. The majority of cells remained entrapped in the splenic parenchyma after injection, while a small number of labeled cells were found in the recipient liver. This is in contrast to rodents, where intrasplenic injection is the preferred route for cell delivery to the liver, and might be due to differences in the microanatomy of the rodent spleen compared with larger mammals (34).

Following intra-arterial infusion, the preferred method for clinical LCT because of the lower risk of medical complications, we observed no MRI signal changes in the spleen, correlating with the small number of liver cells found in the spleen. Therefore, we could not demonstrate considerable hepatization of the spleen, which was previously used as an explanation for the clinical improvements seen after LCT via the intra-arterial route (3,35,36). However, cells were transferred to the liver via the portovenous system, which to date has not been observed in preclinical models of LCT. Histological examination of the liver showed efficient cell engraftment in periportal areas, with microthrombi detected in only two cases. This finding proved the hypothesis that successful engraftment of labeled cells induces no detectable signal changes in liver MRIs. In clinical studies, liver cell engraftment may be further confirmed by proof of metabolic correction or enzymatic activity. The other important issue might be that cell migration from the spleen to the liver led to cell engraftment similar to intraportal infusion, but caused significantly less microembolization detectable by MRI. Thus, cell translocation to the liver could be the leading mechanism responsible for clinical outcomes following LCT to the spleen. The effect may be explained by the gradual clearance of nonattached cells from the spleen via the portovenous system and needs to be further investigated. Our findings are of great clinical importance, because LCT in children with metabolic liver disease is currently performed by intraportal application (11). LCT via the intra-arterial route could enable successful cell engraftment in the liver without microembolization, avoiding the need for a preparative regime and possibly enhancing long-term outcomes of LCT for the treatment of metabolic liver disease. Moreover, this finding should be relevant for stem cell applications to the liver (11,14).

The results of our study are limited by the low number of cells used for transplantation. For MRI monitoring, a fraction of cells should be labeled prior to transplantation. Further studies should investigate the ratio of labeled versus native cells necessary for signal induction by embolized cells. Application of large volumes of liver cells via the intra-arterial route has been shown to cause severe medical complications (23,28), and as a consequence repeated cell infusions with small volumes should be evaluated for clinical applications (19). Another limitation is that we did not investigate possible effects of hepatic damage in our study. As far as clinical relevant disease liver models are available (33), both detectability of cell aggregates as well as cell engraftment after translocation from the spleen will be further investigated.

In conclusion, our study shows that MRI can be a valuable tool for noninvasive elucidation of cellular processes of LCT under clinical conditions. MRI can be used to visualize the microembolization of transplanted liver cells following intraportal infusion, undetectable with conventional noninvasive imaging modalities. Intra-arterial infusion to the spleen leads to efficient translocation of transplanted cells to the liver, while dramatically decreasing the amount of microembolization that is detectable by MRI compared to intraportal application. These findings may be clinically relevant for the treatment of metabolic liver disease, because LCT via the spleen may promote cell engraftment in the liver without significant microembolization, possibly enhancing long-term outcomes of the therapy. Our data suggest that the intra-arterial route deserves further clinical evaluation, with a special focus on cell engraftment within the liver rather than hepatization of the spleen.

ACKNOWLEDGMENTS: The authors are grateful to Dr. Juliane Unger and the team from the Research Institution of Experimental Medicine of the Charité for help with animal care, Dr. Jens Pinkernelle for development of the radiological procedures as well as his knowledge and advice in radiologic experimental design and data evaluation, Kerstin Nehls, Steffen Lippert, and Wiebke Werner for technical assistance, Natalie Schlüter and Elisa Pfeiffer for assistance in the operating room, Virginia Ding-Reinelt for MRI operational assistance, Gabriele Fernahl and Petra Schrade for supporting us with

immunohistology and performing electron microscopy, Tessa Charlotte Lühmann (Department of Materials, ETH Zurich) for performing confocal microscopy, and Dr. Ulrich Gauger for statistical analysis. The study has been supported by grants of the following organizations: CytoNet GmbH, Weinheim, Germany; Fiebig Foundation, Berlin, Germany; European Regional Development Fund (ERDF). Dr. Rüdinger is managing director of CytoNet Gmbh.

REFERENCES

1. Andreoletti, M.; Loux, N.; Vons, C.; Nguyen, T. H.; Lorand, I.; Mahieu, D.; Simon, L.; Di Rico, V.; Vingert, B.; Chapman, J.; Briand, P.; Schwall, R.; Hamza, J.; Capron, F.; Bargy, F.; Franco, D.; Weber, A. Engraftment of autologous retrovirally transduced hepatocytes after intraportal transplantation into nonhuman primates: Implication for ex vivo gene therapy. Hum. Gene Ther. 12(2): 169–179; 2001.
2. Barnett, B. P.; Arepally, A.; Karmarkar, P. V.; Qian, D.; Gilson, W. D.; Walczak, P.; Howland, V.; Lawler, L.; Lauzon, C.; Stuber, M.; Kraitchman, D. L.; Bulte, J. W. Magnetic resonance-guided, real-time targeted delivery and imaging of magnetocapsules immunoprotecting pancreatic islet cells. Nat. Med. 13(8):986–991; 2007.
3. Bilir, B. M.; Guinette, D.; Karrer, F.; Kumpe, D. A.; Krysl, J.; Stephens, J.; McGavran, L.; Ostrowska, A.; Durham, J. Hepatocyte transplantation in acute liver failure. Liver Transpl. 6(1):32–40; 2000.
4. Bos, C.; Delmas, Y.; Desmouliere, A.; Solanilla, A.; Hauger, O.; Grosset, C.; Dubus, I.; Ivanovic, Z.; Rosenbaum, J.; Charbord, P.; Combe, C.; Bulte, J. W.; Moonen, C. T.; Ripoche, J.; Grenier, N. In vivo MR imaging of intravascularly injected magnetically labeled mesenchymal stem cells in rat kidney and liver. Radiology 233(3): 781–789; 2004.
5. Bulte, J. W. In vivo MRI cell tracking: Clinical studies. AJR Am. J. Roentgenol. 193(2):314–325; 2009.
6. Choi, M. S.; Catana, A. M.; Wu, J.; Kim, Y. S.; Yoon, S. J.; Borowsky, A. D.; Gambhir, S. S.; Gupta, S.; Zern, M. A. Use of bioluminescent imaging to assay the transplantation of immortalized human fetal hepatocytes into mice. Cell Transplant. 17(8):899–909; 2008.
7. Dagher, I.; Nguyen, T. H.; Groyer-Picard, M. T.; Lainas, P.; Mainot, S.; Guettier, C.; Pariente, D.; Franco, D.; Weber, A. Efficient hepatocyte engraftment and long-term transgene expression after reversible portal embolization in nonhuman primates. Hepatology 49(3):950–959; 2009.
8. Dhawan, A.; Mitry, R. R.; Hughes, R. D.; Lehec, S.; Terry, C.; Bansal, S.; Arya, R.; Wade, J. J.; Verma, A.; Heaton, N. D.; Rela, M.; Mieli-Vergani, G. Hepatocyte transplantation for inherited factor VII deficiency. Transplantation 78(12):1812–1814; 2004.
9. Dudeck, O.; Bogusiewicz, K.; Pinkernelle, J.; Gaffke, G.; Pech, M.; Wieners, G.; Bruhn, H.; Jordan, A.; Ricke, J. Local arterial infusion of superparamagnetic iron oxide particles in hepatocellular carcinoma: A feasibility and 3.0 T MRI study. Invest. Radiol. 41(6):527–535; 2006.
10. Fisher, R. A.; Strom, S. C. Human hepatocyte transplantation: Worldwide results. Transplantation 82(4):441–449; 2006.
11. Fitzpatrick, E.; Mitry, R. R.; Dhawan, A. Human hepatocyte transplantation: State of the art. J. Intern. Med. 266(4):339–357; 2009.
12. Grossman, M.; Raper, S. E.; Kozarsky, K.; Stein, E. A.; Engelhardt, J. F.; Muller, D.; Lupien, P. J.; Wilson, J. M. Successful ex vivo gene therapy directed to liver in a patient with familial hypercholesterolaemia. Nat. Genet. 6(4):335–341; 1994.
13. Gupta, S.; Rajvanshi, P.; Sokhi, R.; Slehria, S.; Yam, A.; Kerr, A.; Novikoff, P. M. Entry and integration of transplanted hepatocytes in rat liver plates occur by disruption of hepatic sinusoidal endothelium. Hepatology 29(2):509–519; 1999.
14. Haridass, D.; Narain, N.; Ott, M. Hepatocyte transplantation: Waiting for stem cells. Curr. Opin. Organ Transplant. 13(6):627–632; 2008.
15. Ju, S.; Teng, G. J.; Lu, H.; Zhang, Y.; Zhang, A.; Chen, F.; Ni, Y. In vivo MR tracking of mesenchymal stem cells in rat liver after intrasplenic transplantation. Radiology 245(1):206–215; 2007.
16. Khan, A. A.; Shaik, M. V.; Parveen, N.; Rajendraprasad, A.; Aleem, M. A.; Habeeb, M. A.; Srinivas, G.; Raj, T. A.; Tiwari, S. K.; Kumaresan, K.; Venkateswarlu, J.; Pande, G.; Habibullah, C. M. Human fetal liver-derived stem cell transplantation as supportive modality in the management of end-stage decompensated liver cirrhosis. Cell Transplant. 19(4):409–418; 2010.
17. Maruyama, M.; Totsugawa, T.; Kunieda, T.; Okitsu, T.; Shibata, N.; Takesue, M.; Kurabayashi, Y.; Oshita, M.; Nakaji, S.; Kodama, M.; Tanaka, N.; Kobayashi, N. Hepatocyte isolation and transplantation in the pig. Cell Transplant. 12(6):593–598; 2003.
18. Medarova, Z.; Vallabhajosyula, P.; Tena, A.; Evgenov, N.; Pantazopoulos, P.; Tchipashvili, V.; Weir, G.; Sachs, D.; Moore, A. In vivo imaging of autologous islet grafts in the liver and under the kidney capsule in non-human primates. Transplantation 87(11):1659–1666; 2009.
19. Meyburg, J.; Das, A. M.; Hoerster, F.; Lindner, M.; Kriegbaum, H.; Engelmann, G.; Schmidt, J.; Ott, M.; Pettenazzo, A.; Luecke, T.; Bertram, H.; Hoffmann, G. F.; Burlina, A. One liver for four children: First clinical series of liver cell transplantation for severe neonatal urea cycle defects. Transplantation 87(5):636–641; 2009.
20. Modo, M. Noninvasive imaging of transplanted cells. Curr. Opin. Organ Transplant. 13(6):654–658; 2008.
21. Modo, M.; Meade, T. J.; Mitry, R. R. Liver cell labelling with MRI contrast agents. Methods Mol. Biol. 481:207–219; 2009.
22. Muraca, M.; Neri, D.; Parenti, A.; Feltracco, P.; Granato, A.; Vilei, M. T.; Ferraresso, C.; Ballarin, R.; Zanusso, G. E.; Giron, G.; Rozga, J.; Gerunda, G. Intraportal hepatocyte transplantation in the pig: Hemodynamic and histopathological study. Transplantation 73(6):890–896; 2002.
23. Nagata, H.; Ito, M.; Shirota, C.; Edge, A.; McCowan, T. C.; Fox, I. J. Route of hepatocyte delivery affects hepatocyte engraftment in the spleen. Transplantation 76(4): 732–734; 2003.
24. Ponder, K. P.; Gupta, S.; Leland, F.; Darlington, G.; Finegold, M.; DeMayo, J.; Ledley, F. D.; Chowdhury, J. R.; Woo, S. L. Mouse hepatocytes migrate to liver parenchyma and function indefinitely after intrasplenic transplantation. Proc. Natl. Acad. Sci. USA 88(4):1217–1221; 1991.
25. Quaglia, A.; Lehec, S. C.; Hughes, R. D.; Mitry, R. R.; Knisely, A. S.; Devereaux, S.; Richards, J.; Rela, M.; Heaton, N. D.; Portmann, B. C.; Dhawan, A. Liver after hepatocyte transplantation for liver-based metabolic disorders in children. Cell Transplant. 17(12):1403–1414; 2008.
26. Raschzok, N.; Billecke, N.; Kammer, N. N.; Morgul, M. H.; Adonopoulou, M. K.; Sauer, I. M.; Florek, S.;

Becker-Ross, H.; Huang, M. D. Quantification of cell labeling with micron-sized iron oxide particles using continuum source atomic absorption spectrometry. Tissue Eng. Part C Methods 15(4):681–686; 2009.
27. Raschzok, N.; Morgul, M. H.; Pinkernelle, J.; Vondran, F. W.; Billecke, N.; Kammer, N. N.; Pless, G.; Adonopoulou, M. K.; Leist, C.; Stelter, L.; Teichgraber, U.; Schwartlander, R.; Sauer, I. M. Imaging of primary human hepatocytes performed with micron-sized iron oxide particles and clinical magnetic resonance tomography. J. Cell. Mol. Med. 12(4):1384–1394; 2008.
28. Rosenthal, R. J.; Chen, S. C.; Hewitt, W.; Wang, C. C.; Eguchi, S.; Geller, S.; Phillips, E. H.; Demetriou, A. A.; Rozga, J. Techniques for intrasplenic hepatocyte transplantation in the large animal model. Surg. Endosc. 10(11):1075–1079; 1996.
29. Schwartlander, R.; Schmid, J.; Brandenburg, B.; Katenz, E.; Vondran, F. W.; Pless, G.; Cheng, X.; Pascher, A.; Neuhaus, P.; Sauer, I. M. Continuously microscopically observed and process-controlled cell culture within the SlideReactor: Proof of a new concept for cell characterization. Tissue Eng. 13(1):187–196; 2007.
30. Shapiro, E. M.; Sharer, K.; Skrtic, S.; Koretsky, A. P. In vivo detection of single cells by MRI. Magn. Reson. Med. 55(2):242–249; 2006.
31. Shi, X. L.; Gu, J. Y.; Han, B.; Xu, H. Y.; Fang, L.; Ding, Y. T. Magnetically labeled mesenchymal stem cells after autologous transplantation into acutely injured liver. World J. Gastroenterol. 16(29):3674–3679; 2010.
32. Slotkin, J. R.; Cahill, K. S.; Tharin, S. A.; Shapiro, E. M. Cellular magnetic resonance imaging: nanometer and micrometer size particles for noninvasive cell localization. Neurotherapeutics 4(3):428–433; 2007.
33. Soltys, K. A.; Soto-Gutierrez, A.; Nagaya, M.; Baskin, K. M.; Deutsch, M.; Ito, R.; Shneider, B. L.; Squires, R.; Vockley, J.; Guha, C.; Roy-Chowdhury, J.; Strom, S. C.; Platt, J. L.; Fox, I. J. Barriers to the successful treatment of liver disease by hepatocyte transplantation. J. Hepatol. 53(4):769–774; 2010.
34. Steiniger, B.; Barth, P.; Herbst, B.; Hartnell, A.; Crocker, P. R. The species-specific structure of microanatomical compartments in the human spleen: Strongly sialoadhesin-positive macrophages occur in the perifollicular zone, but not in the marginal zone. Immunology 92(2):307–316; 1997.
35. Sterling, R. K.; Fisher, R. A. Liver transplantation. Living donor, hepatocyte, and xenotransplantation. Clin. Liver Dis. 5(2):431–460; 2001.
36. Strom, S. C.; Fisher, R. A.; Thompson, M. T.; Sanyal, A. J.; Cole, P. E.; Ham, J. M.; Posner, M. P. Hepatocyte transplantation as a bridge to orthotopic liver transplantation in terminal liver failure. Transplantation 63(4):559–569; 1997.
37. Vons, C.; Loux, N.; Simon, L.; Mahieu-Caputo, D.; Dagher, I.; Andreoletti, M.; Borgnon, J.; Di Rico, V.; Bargy, F.; Capron, F.; Weber, A.; Franco, D. Transplantation of hepatocytes in nonhuman primates: A preclinical model for the treatment of hepatic metabolic diseases. Transplantation 72(5):811–818; 2001.
38. Weissleder, R.; Cheng, H. C.; Bogdanova, A.; Bogdanov, Jr., A. Magnetically labeled cells can be detected by MR imaging. J. Magn. Reson. Imaging 7(1):258–263; 1997.
39. Yamanouchi, K.; Zhou, H.; Roy-Chowdhury, N.; Macaluso, F.; Liu, L.; Yamamoto, T.; Yannam, G. R.; Enke, C.; Solberg, T. D.; Adelson, A. B.; Platt, J. L.; Fox, I. J.; Roy-Chowdhury, J.; Guha, C. Hepatic irradiation augments engraftment of donor cells following hepatocyte transplantation. Hepatology 49(1):258–267; 2009.